J Electroceram (2011) 27:134–142
DOI 10.1007/s10832-011-9658-3

Oxygen incorporation in porous thin films of strontium doped lanthanum ferrite

Martin Søgaard · Anja Bieberle-Hütter · Peter Vang Hendriksen · Mogens Mogensen · Harry Louis Tuller

Received: 22 July 2011 / Accepted: 12 October 2011 / Published online: 4 November 2011

Abstract Electrical conductivity relaxation measurements were carried out on thin films of $(La_{0.6}Sr_{0.4})_{0.99}FeO_{3-\delta}$ deposited on MgO (100) substrates by pulsed laser deposition in order to determine the surface exchange coefficient, k_{Ex}, of the oxygen incorporation process in the temperature range 550–700°C. The composition of the films was verified using wavelength dispersive x-ray and Rutherford backscattering spectroscopy. Scanning electron microscopy showed small triangular crystallites with the largest dimension 80 nm and the smallest dimension 10 nm. X-ray diffraction showed a cubic perovskite structure and significant texturing. At a constant temperature, k_{Ex} was found to be a function only of the final p_{O_2} of the p_{O_2}-changes the sample was subjected to during conductivity relaxation experiments, confirming that the magnitude of the exchange coefficient was not influenced by changes in ionic defect concentrations. The k_{Ex}-values determined for these thin films were significantly lower than for bulk samples. A value of 3.6×10^{-6} cm s^{-1} was obtained at 702°C and a final p_{O_2} of 0.048 atm, approximately a factor of six lower than that obtained for bulk samples. An activation energy of 282 ± 20 kJ mol^{-1} was found for the surface exchange coefficient at $p_{O_2} = 0.048$ atm. Possible reasons for the reduced magnitude of k_{Ex} are discussed including the role of thermal history in influencing surface morphology and chemistry.

Keywords Thin film · LSF · Conductivity relaxation · Solid oxide fuel cells · Oxygen reduction kinetics · Sensors

1 Introduction

Perovskites in the system $(La_{1-x}Sr_x)_sCo_{1-y}Fe_yO_{3-\delta}$ (with $s \approx 1$) show a high oxide ion- and electronic conductivity at high temperatures and high oxygen partial pressures. They are therefore of interest for applications as oxygen separation membranes, cathodes for solid oxide fuel cells (SOFCs) and sensors. For a SOFC-stack, lowering the operating temperature to the range 550–650°C will increase the likelihood of widespread commercialization of the technology, as less costly steels can be used for interconnects and supports. However, the minimum operation temperature will still be limited by the temperature at which the electrode kinetics limit the overpotential losses to an acceptable level [1–3]. It is therefore important to obtain information on the kinetics of oxygen incorporation into perovskite type oxides at temperatures expected to become relevant operating temperatures for SOFCs. Recently, thin film electrodes have drawn increasing interest as components of thin film or micro

M. Søgaard (✉) · P. V. Hendriksen · M. Mogensen
Risø National Laboratory for Sustainable Energy,
Fuel Cells and Solid State Chemistry Division,
Technical University of Denmark, Frederiksborgvej 399,
P.O. Box 49, 4000 Roskilde, Denmark
e-mail: msqg@risoe.dtu.dk

A. Bieberle-Hütter
Nonmetallic Inorganic Materials, ETH Zurich,
Wolfgang-Pauli-Str. 10, 8093 Zürich, Switzerland

H. L. Tuller
Crystal Physics and Electroceramics Laboratory,
Department of Materials Science and Engineering,
Massachusetts Institute of Technology, Cambridge,
MA 02139, USA

fuel cell structures offering reduced temperature and/or portable operation [4–8].

To date, only few studies have attempted to determine the kinetic parameters of thin film (TF) Mixed Ionic Electronic Conducting (MIEC) perovskites. Chen et al. [9] investigated the oxygen incorporation kinetics by conductivity relaxation of an epitaxial $La_{0.5}Sr_{0.5}CoO_{3-\delta}$ TF grown by pulsed laser deposition (PLD). A main conclusions of the study was that the surface exchange coefficient, k_{Ex}, was independent of the initial p_{O_2}, but depended only on the final p_{O_2} of the p_{O_2}-changes the sample was exposed to. If the film was annealed at 900°C, the value of k_{Ex} increased substantially with the increase reported to be associated with a change in the film surface. The surface exchange coefficient increased with increasing temperature with an (here estimated) activation energy of 168 kJ mol^{-1}.

Hole et al. [10] investigated the electrical response of TF $LaFeO_{3-\delta}$ upon changes in oxygen partial pressure. A significant *p*-type contribution was measured at 1000°C and $p_{O_2} > 10^{-10}$ atm, likely originating either from back ground impurities (aliovalent) or from cation vacancies in $LaFeO_3$ as described by Wærnhus [11].

Baumann et al. [12] investigated TF microelectrodes of $La_{0.6}Sr_{0.4}Co_{0.8}Fe_{0.2}O_{3-\delta}$ using impedance spectroscopy. It was shown that the electrochemical resistance towards oxygen reduction was dominated by the oxygen exchange reaction at the surface of the electrode.

Mosleh et al. investigated $(La_{0.6}Sr_{0.4})_{0.99}FeO_{3-\delta}$ TFs deposited on MgO (100) single crystals using PLD [13, 14]. The film microstructure was characterised and the electrical conductivity as well as the exchange kinetics studied as a function of p_{O_2} and temperature. It was found that a long annealing time (>300 h) at 950°C was necessary to obtain stable values of the electrical conductivity at temperatures below 950°C. During this annealing a structural relaxation of the TF took place. Figure 1 shows a schematic of this relaxation. The pre-annealed film consisted of a dense film with an approximate thickness of 150 nm with columnar grains rising from this film surface. These grains were often separated by a small space of few nanometers. During the annealing, grain growth resulted in the closing of these tiny gaps leaving a TF with larger closed porosities.

Figure 1 also illustrates that the electrochemically active area, A_s, can be many times larger than the geometrical area that the film has been deposited onto (A_g). In studies on $La_{0.58}Sr_{0.4}Co_{0.8}Fe_{0.2}O_{3-\delta}$ by Plonczak et al. [7] it was shown that by tailoring of the PLD deposition parameters an increase in electrochemical active area, A_s/A_g, of a factor of 26 for a 680 nm film was feasible. It should in this respect be noted that A_s/A_g for a typical SOFC cathode prepared using conventional techniques (i.e. screen printing and sintering) is approximately 10–200. These numbers have been estimated using conventional particle sizes (100 nm–2 μm) and thicknesses of cathodes (1–50 μm). In addition, the oxide ions in a typical cathode are transported through many grains in a circuitous path, resulting in additional resistance. This highlights the possibilities of using tailored thin films as highly efficient cathodes for solid oxide fuels cells as a large surface area can be combined with a short direct diffusion path.

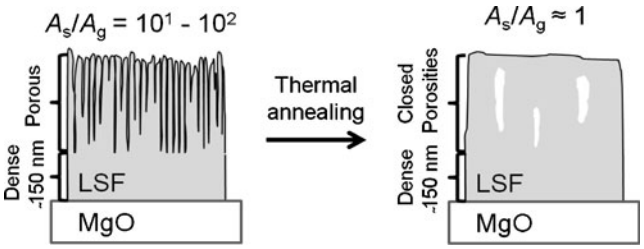

Fig. 1 Schematic of the cross sections after deposition (*left*) and after thermal annealing (*right*). A_s is the electrochemical active area area of the thin film and A_g is the geometrical area onto which the film is deposited

The motivation of this study was to investigate the properties of perovskites at temperatures relevant for operation of future generations of SOFCs, ie. 550°C. As in the study by Mosleh et al. we study TFs of $(La_{0.6}Sr_{0.4})_{0.99}FeO_{3-\delta}$ (LSF) prepared using PLD on single crystals of MgO. Contrary to the study of Mosleh et al. [13, 14] we investigate the surface exchange kinetics on samples that have not undergone the structural relaxation shown in Fig. 1. The TFs have been thoroughly characterized using a variety of techniques. Moreover, when the material is studied in the form of TFs, the surface exchange kinetics can be assessed without interference from bulk diffusion leading to high accuracy.

2 Theory: Electrical conductivity relaxation

Electrical conductivity relaxation (ECR) is a well established method for determining the oxygen transport properties of MIECs [11, 15–17]. Upon a change in the oxygen partial pressure, the sample changes oxygen stoichiometry leading as well to a change in charge carrier concentration. A change in the charge carrier concentration is reflected as a change in the electronic conductivity.

A schematic of a thin film sample as used in this study is shown in Fig. 2. The dimension in the x— direction is much smaller than the dimensions in the $y-$ and $z-$ direction of the thin film. The diffusion can therefore be approximated by a 1-dimensional problem.

When correlating the response of the electrical conductivity to Fick's laws of diffusion, one can determine a chemical diffusion coefficient, D_{Chem}, and a surface exchange coefficient, k_{Ex}. By fitting the response of the electrical conductivity as a function of time to Eq. 1, D_{Chem} and k_{Ex} can be obtained [15–20].

$$\frac{\sigma(\infty)-\sigma(t)}{\sigma(\infty)-\sigma(0)}=\sum_{n=1}^{\infty}\frac{2L_x^2\exp\left(\frac{-\beta_{n,x}^2 D_{\mathrm{Chem}}t}{(2l_x)^2}\right)}{\beta_{n,x}^2(\beta_{n,x}^2+L_x^2+L_x)} \tag{1}$$

$\sigma(0)$ is the conductivity prior to the gas change and $\sigma(\infty)$ is the steady state value after the change. $\sigma(t)$ is the conductivity at time t. The gas change is assumed to be infinitely fast and to occur at $t=0$. l_x is half the thickness of the sample and it is assumed that oxygen can only penetrate from one surface. The other surface is assumed impermeable (substrate/MIEC interface). $\beta_{n,x}$ is the n'th positive root to the equation

$$\beta_{n,x}\tan\beta_{n,x}=L_x \tag{2}$$

where L_x is the dimensionless parameter

$$L_x=\frac{2l_x k_{\mathrm{Ex}}}{D_{\mathrm{Chem}}} \tag{3}$$

The assumptions needed for Eq. 1 to be valid are: (i) local electro-neutrality (ii) proportionality between the charge carrier concentration and the electrical conductivity (iii) a surface exchange reaction of first order, and (iv) a constant diffusion coefficient between the initial and final p_{O_2}. The first order surface reaction can be described by Eq. 4.

$$J=-D_{\mathrm{Chem}}\frac{\partial C(\pm l_x,t)}{\partial x}=k_{\mathrm{Ex}}\big(C(\pm l_x,t)-C(\pm l_x,\infty)\big) \tag{4}$$

J is the flux of oxygen ions from the surface to the bulk and $C(l_x,t)$ represents the concentration of oxide ions at the surface to time t and $C(l_x,\infty)$ represents the equilibrium concentration of oxygen ions ($t=\infty$). In order to fulfill the conditions (ii) to (iv), the change in oxygen partial pressure should be small corresponding to a small change in the vacancy concentration compared to the absolute vacancy concentration.

The characteristic thickness, L_c, can be calculated from $L_c=D_{\mathrm{Chem}}/k_{\mathrm{Ex}}$, and defines the thickness at which a given driving force distributes equally over the surface reaction and bulk diffusion [21]. For a sample with a thickness of 500 nm and assuming that $k_{\mathrm{Ex}}=10^{-7}$ cm s^{-1}, the value of D_{Chem} needs to be by far less than 10^{-11} cm^2 s^{-1} in order to change the relaxation from mainly surface limited to diffusion limited. A value of $D_{\mathrm{Chem}}=10^{-11}$ cm^2 s^{-1} is found at approximately 300°C (extrapolated from Søgaard et al. [22]). This temperature is far below that which has been examined in this study. Given the small thickness examined in this study, the relaxations will not be influenced by the chemical diffusion coefficient.

If only surface exchange limits the oxygen incorporation (Eq. 1) reduces to [17]

$$\frac{\sigma(\infty)-\sigma(t)}{\sigma(\infty)-\sigma(0)}=\exp\left(-\frac{k_{\mathrm{Ex}}t}{2l_x}\right) \tag{5}$$

Oxygen incorporation into the perovskite matrix is thus described using a single exponential function.

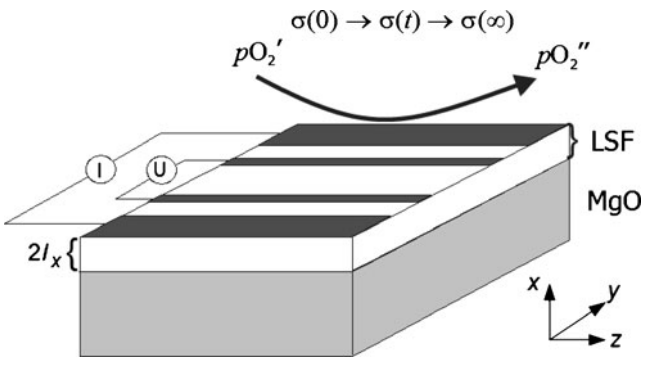

Fig. 2 Schematic of the sample on an MgO-substrate. The thickness of the TF is grossly exaggerated when compared to the thickness of the substrate

3 Experimental

Samples were prepared by depositing LSF on MgO (100) single crystalline substrates using PLD. The substrate size was 1 × 1 cm. The nominal composition of the target was $(La_{0.6}Sr_{0.4})_{0.99}FeO_{3-\delta}$. MgO was used as the substrate in order to avoid reaction between the substrate and the thin film [23]. Powder for the PLD target was prepared using a glycine-nitrate synthesis as described by Chick et al. [24]. Calcined powder was pressed uni-axially and sintered at 1200°C for 20 h. Deposition was performed at a substrate temperature of 550°C in order to ensure the crystallinity of the TF. A pressure of 1.32×10^{-4} atm pure oxygen

was maintained in the chamber to ensure that the film was not heavily reduced. Three samples were prepared under identical conditions but with different deposition times. For the samples with 15, 30 and 45 min deposition times, the abbreviations LSF(a), (b) and (c) are used, respectively. After deposition the thin films were characterized using scanning electron microscopy (SEM) (FEI/Philips XL30 FEG ESEM).

The film thickness was measured with a Tencor P10 profilometer and was averaged over seven measurements with the uncertainty corresponding to three times the standard deviation.

After deposition, all three films had a yellow/brown color, contrary to the normal black color of the perovskite. The brown color is assumed to originate from a tri-valent state of all the iron ions. The composition of the film after deposition is thus $(La_{0.6}Sr_{0.4})_{0.99}FeO_{2.787}$ assuming that 1% cation vacancies are still present in the TF. This will be referred to as the thin film is in a *reduced* state. Subsequent annealing in air resulted in significantly different properties such as color and high electrical conductivity due to oxidation of the film. In this state the film will be referred to as being *oxidized*.

Visible light absorption and thickness of the sample LSF(c) (in the reduced state) were measured at room temperature in air using a spectroscopic ellipsometer (Sopra GES5 UV-VIS-IR).

X-ray diffraction was carried out using a Rigaku 185 nm Bragg Brentano Diffractometer equipped with a rotating Cu-anode. The diffraction pattern showed a highly oriented film with no peak splitting.

Wavelength dispersive x-ray spectroscopy (WDS) (JEOL JXA-733) was carried out on the thickest of the samples (LSF(c)). Rutherford backscattering spectroscopy (RBS) was carried out on the thinnest of the samples (LSF(a)).

Samples were masked with vacuum tape such that four Au-probes could be sputtered onto the film. Figure 2 shows a schematic of the TF with the four Au-probes. A current of approximately 0.5 mA was applied between the two end electrodes leading to an electrical potential difference between the two middle electrodes of approximately 100 mV.

The samples LSF(a) and LSF(b) were investigated on a hot stage (Linkam Instruments TMS94) where electrical contacts to the sample were made using a microprobe station (Karl Suss PM5) and tungsten probes (Karl Suss). For the hot stage measurements the heating rate was approximately 10°C min^{-1} and the hold time at each point was 10 min. Sample LSF(b) was also tested in a tube furnace. Sample LSF(c) was tested thoroughly in a different tube furnace where the oxygen partial pressure was varied between 1 atm to 10^{-3} atm. A more detailed description of the tube furnace can be found in Søgaard et al. [25] . In the test of LSF(c) in the tube furnace, the sample chamber is small compared to the flow rate of the gases. The change in conductivity as a function of time can thus, be correlated to a surface exchange coefficient. It should be noted that no kinetic information could be obtained above 700°C, since the time response of the electrical conductivity was similar to the time response of the external oxygen sensor revealing that the response time was limited by the time needed to displace the gas in the chamber.

4 Results and discussion

4.1 Thickness and composition

Table 1 lists the thickness and summarizes the characterization methods performed on each sample.

Wavelength dispersive spectroscopy indicated the composition $La_{0.73}Sr_{0.46}FeO_x$, where x signifies that the oxygen concentration is unknown. The La/Sr-ratio was measured to be 1.6 which is close to the target composition of 1.5. It is unlikely that the film can have an excess of La and Sr on the A-site of this magnitude without forming secondary phases detectable in XRD. Hence, the apparent 19% A-site excess is ascribed to measurement uncertainties.

Analysis of the data obtained using Rutherford backscattering spectroscopy gave a nominal composition of $La_{0.55}Sr_{0.44}FeO_x$, where x signifies that the oxygen concentration is unknown. The composition measured with RBS is thus very close to the target composition. The thickness measured from RBS was 326 nm, which is consistent with the 280 ± 66 nm

Table 1 Thickness, $2l_x$, as measured by a profilometer (PM) and characterization performed on each sample

Sample	$2l_x$(PM) [nm]	$2l_x$ (RBS) [nm]	$2l_x$ (AS) [nm]	Experiments
LSF(a)	280 ± 66	326		EC, RBS
LSF(b)	500 ± 60			EC, ECR
LSF(c)	570 ± 120		737	EC, ECR, AS, WDS

The uncertainty is three times the standard deviation
EC Electrical Conductivity, *ECR* Electrical Conductivity Relaxation, *AS* Absorption Spectroscopy, *RBS* Rutherford Backscattering Spectroscopy, *WDS* Wavelength Dispersive x-ray Spectroscopy

measured by profilometry. Hence, both techniques lead to similar results.

The thickness of sample LSF(c) calculated from the absorption spectrum was (737 ± 7) nm. Spectroscopic ellipsometer measurements were performed across a large area of the film, whereas the profilometer measurements were limited to the edges of the film.

4.2 SEM investigations

Figure 3 shows an SEM image of sample LSF(c) before the initial heating. Many small triangular/pyramid-shaped crystallites are observed. The largest crystallite dimension is approximately 80 nm while the smallest is approximately 10 nm.

After heating and electrochemical testing at high temperature the surface morphology was investigated again by SEM. A similar grain structure was found, however, the grains had grown and had more rounded edges as compared to the ones in Fig. 3.

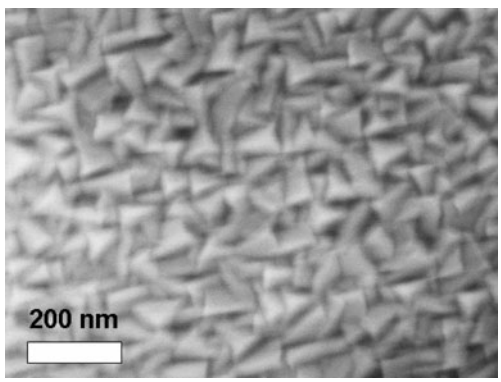

Fig. 3 SEM *top view* image of the sample LSF(c) after deposition at 550°C and prior to the electrochemical measurements. After the electrochemical measurements, the sample had a similar grain structure but with more rounded edges

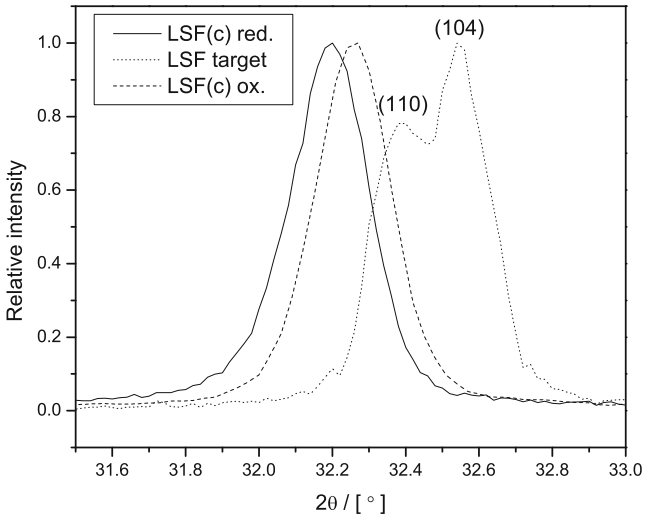

Fig. 4 Comparison of x-ray diffractograms of the target and TF for the (110)/(104)-peaks. The reduced (*red.*) State of the TF is the *solid line* and the oxidized state (*ox.*) is the *dashed line*

4.3 X-ray diffraction

Figure 4 shows the x-ray diffraction pattern of the target used for preparing the films in the range $31.5 < 2\theta < 33.0$ (dotted line) and the TF in both the reduced (solid line) and oxidized state (dashed line). For the target, the (110) and (104) peaks are clearly seen. The peaks for the film in both the reduced and oxidized state show no sign of splitting. This indicates that the film has crystallized and remains in the cubic structure. Assuming a hexagonal setting (as for the target), the peaks originating from the film were attributed to the planes (110)/(104), (300)/(214)/(018), and (220)/(208). Assuming a cubic phase, the peaks can be attributed to (110), (210) and (220).

A pseudo cubic lattice constant can be calculated from the diffractograms; a value of $a_c = 3.899$ is found for the target, and a cubic lattice constant for the reduced state of the film to $a_c = 3.929$ Å, corresponding to a film strain of $\epsilon = 0.76\%$. The cubic lattice constant for the film in the oxidized state is $a_c = 3.921$ Å leading to a strain of $\epsilon = 0.57\%$ when compared to the target. Upon annealing, the films take up oxygen and an increase in the oxygen content causes the material to contract [26–28] consistent with the above lattice parameters. According to the results of Mosleh et al. [14] it seems reasonable to assume that the film is completely oxidized such that $\delta \approx 0.00$. A significant strain is thus still present in the film compared to the target.

4.4 Optical absorption measurements of sample LSF(c) in the reduced state

Figure 5 shows the optical absorption of the as-deposited sample as a function of the energy of the incident photons. A band edge is observed at approximately 2.1 eV in accordance with the yellow/brownish color of the sample.

In Fig. 5, two features at 3.1 eV and 3.8 eV are prominent. According to Chainani et al. [29], the peaks at 3.1 eV and 3.8 eV must be assigned to transitions from the valence band into the $t_{2g\downarrow}$ and $e_{g\downarrow}$ levels,

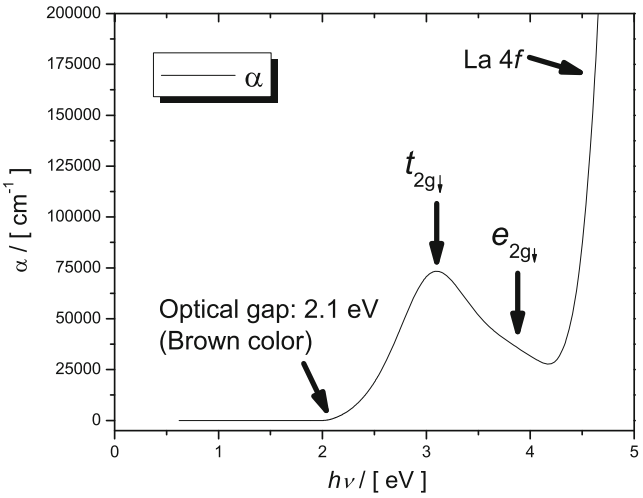

Fig. 5 Optical absorption spectrum of sample LSF(c) prior to heating. The different transitions from the valence band into the unoccupied Fe 3d- states are marked in the figure

respectively. The large feature at 4.5 eV is assigned to La 4*f* states. No spectral intensity is observed at the Fermi level consistent with the insulating properties at low temperature. Chainani et al. also observed a feature at 1.2 eV above the Fermi level for Sr-doped $LaFeO_{3-\delta}$ which was attributed to transitions from the valence band to the $e_{g\uparrow}$ state. This feature is not observed in our absorption spectrum since the sample is in the reduced state, where the Fe 3*d* configuration is $t^3_{2g\uparrow}e^2_{g\uparrow}$. Transitions into the $e_{g\uparrow}$ level is thus not possible. The optical spectrum thus strongly supports the assumption that the TF is oxygen deficient right after deposition. Also an electronic structure similar to $LaFeO_3$ is obtained.

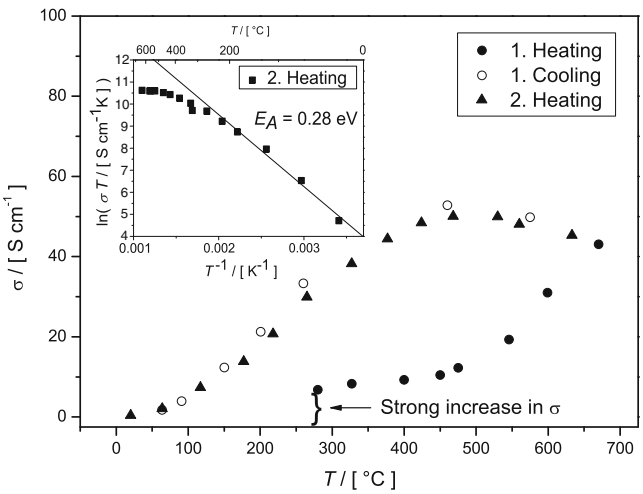

Fig. 6 Electrical conductivity in air upon heating and cooling sample LSF(b) on the hot stage. The inset in Fig. 6 shows $\ln(\sigma T)$ as a function of the reciprocal absolute temperature. The activation energy for electronic conduction is shown

4.5 Electrical conductivity measurements

Figure 6 shows the electrical conductivity for LSF(b) upon heating and cooling the TF in air. The electrical conductivity was not measurable at room temperature before the first heating. Upon heating, the conductivity increased orders of magnitude at approximately 250°C, which is marked in the figure. At the same time the film changed color from dark yellow to black.

When cooling, the conductivity was not reversible but remained at a significantly higher level than when heating, and the film remained black. The second heating was similar to the first cooling. We have estimated the uncertainty of the electrical conductivity to be 25%, mainly due to the uncertainty in the thickness of the film. The strong increase in conductivity at 250°C is attributed to oxygen incorporation into the perovskite resulting in the formation of *p*-type charge carriers (electron-holes). This transition is thus where the film is transformed from the *reduced* to the *oxidized* state.

The inset in Fig. 6 shows a plot of $\ln \sigma T$ vs. T^{-1} exhibiting an activation energy of 0.28 ± 0.05 eV in the low temperature range ($T < 200$°C). Mosleh et al. determined an activation energy of 0.31 eV [13] where the bulk material is 0.30 eV. Our value of the activation energy is thus in good agreement with both the values determined for a bulk sample and TFs.

Table 2 shows the maximum conductivity, σ_{Max}, and the temperature at which σ_{Max} is obtained for the three different samples. It should be noted that samples LSF(a) and (b) were measured on a hot stage with some uncertainty on the actual temperature, while sample LSF(c) was measured in a furnace where the temperature was very constant. For a bulk sample, we have measured $\sigma_{\mathrm{Max}} = 228$ S cm^{-1} at 579°C [22]. The reason for the higher conductivity for LSF(a) can be understood from Fig. 1. As a larger part of the thinnest film (LSF(a)) is dense compared to the thicker films (LSF(b) and LSF(c)), this also results in an apparent

Table 2 Maximum measured conductivity, σ_{Max}, and the temperature for, σ_{Max}, for the three investigated samples

	T/[°C]	σ_{Max}/[S cm^{-1}]
LSF(a) (280 ± 66 nm)	482	82
LSF(b) (500 ± 60 nm)	490	50
LSF(c) (570 ± 120 nm)	615	39
LSF(bulk)	579	228

The thicknesses of the films are also listed (profilometer). Values for a bulk sample are also shown

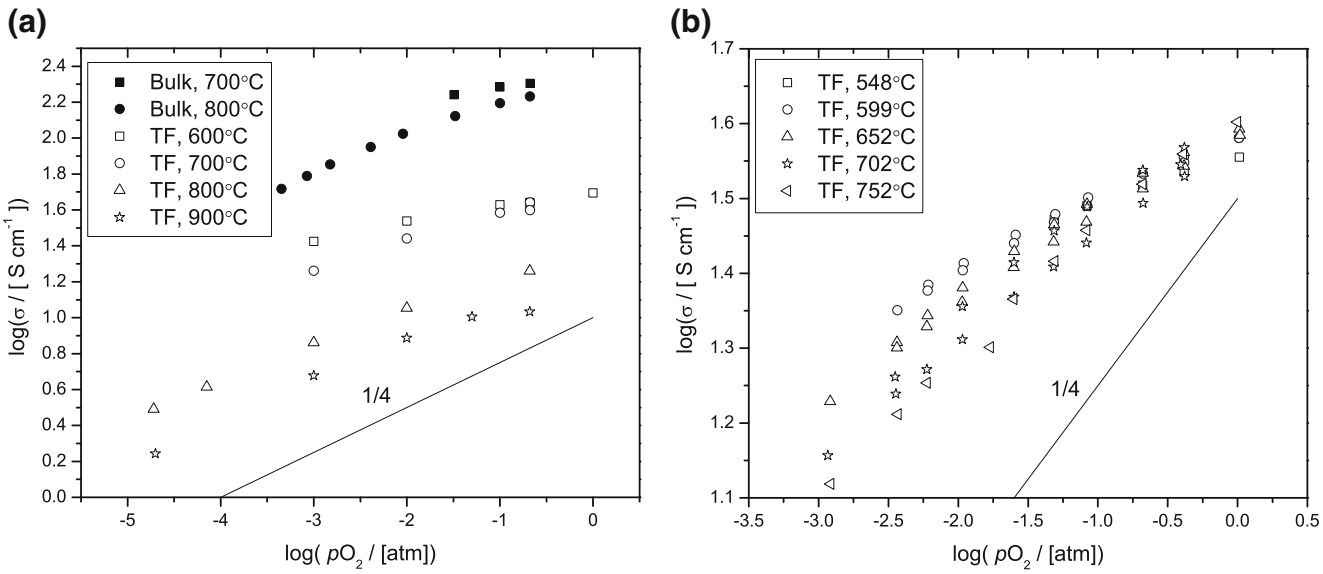

Fig. 7 (**a**) Equilibrium electrical conductivity measurements for sample LSF(b). (**b**) Equilibrium electrical conductivity measurements for sample LSF(c)

conductivity that is higher. Comparing the thickness (Table 1) with the value of the maximum conductivity (Table 2) it actually seems that the porous part of the film does not contribute significantly to the conductance of the sample, consistent with the fact that the porosities are located perpendicular to the current path.

Figure 7(a) and (b) shows the logarithm of the conductivity as a function of $\log(p_{O_2})$ for sample LSF(b) and LSF(c), respectively. Bulk values from Søgaard et al. [22] are also shown in Fig. 7(a). The values of the conductivity measured in the furnace at 600 and 700°C are seen to be consistent with those measured on the hot stage (Figs. 7(a) and 6).

From Fig. 7(a) and (b) it is seen that the conductivities at 600 and 700°C for the films are very similar. With increasing temperature, the conductivity decreases at a constant p_{O_2}. This decrease is attributed to an increasing oxygen vacancy concentration and the associated loss of p-type charge carriers. A slope of 1/4 expected for large values of δ is illustrated in the figure. The samples approach this p_{O_2}-dependence only at high temperature and low p_{O_2}.

The sample LSF(b) was heated to 800°C and 900°C and subjected to changes in the p_{O_2}. Short equilibration times were used when measuring the conductivity for sample LSF(b) as it was observed that the conductivity of the sample was not completely reversible, especially at the high temperatures. Therefore the maximum temperature of sample LSF(c) was kept below 752°C. However, despite the relatively low temperature, the initial conductivity in oxygen (p_{O_2}=1.0 atm) at 752°C was 40.0 S cm^{-1} but when returning to oxygen (from a $p_{O_2} = 1.2 \times 10^{-3}$ atm), the conductivity dropped to 33.2 S cm^{-1}, which is a decrease of 17%. This suggests possible degradation in the film, morphology changes or interaction with the substrate.

4.6 Electrical conductivity relaxation

Figure 8 shows a typical conductivity relaxation at 702°C. Also shown is a fit with a single exponential function (dotted line), which assumes that only one

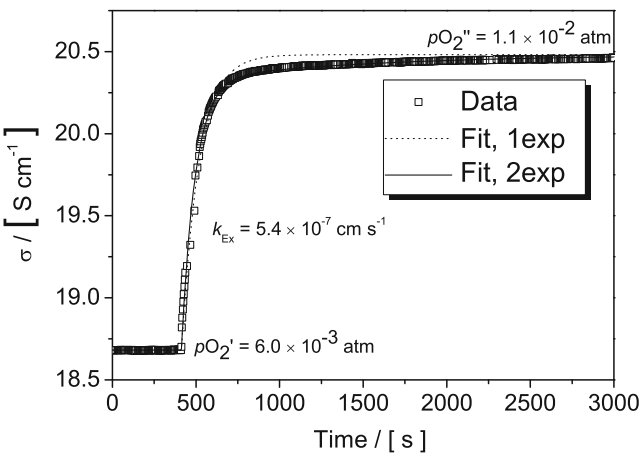

Fig. 8 Electrical conductivity of sample LSC(c) upon a change in p_{O_2}. The relaxation was fitted with a single exponential function (Eq. 5) and with two exponential functions (Eq. 6), respectively

process (oxygen incorporation) contributes to the relaxation process.

The measured relaxations can be fitted with a single exponential function, however, it is observed that the fitting is not satisfactory at long times. In order to describe the measured relaxations more accurately, we have therefore assumed that one additional process is occurring. We have chosen to describe this second relaxation with one more exponential function according to the equation:

$$\frac{\sigma(\infty)-\sigma(t)}{\sigma(\infty)-\sigma(0)} = A_1 \exp\left(-\frac{k_{Ex}t}{2l_x}\right) + A_2 \exp\left(-\frac{t}{\tau_2}\right) \quad (6)$$

Where the condition $A_1 + A_2 = 1$ applies. For the relaxation shown in Fig. 8 the following parameters where obtained: $A_1 = 0.922$, $A_2 = 0.078$, $\tau_2 = 1221$ s. τ_2 is typically in the range 1,000–20,000 s and showed thermal activation. The second term in Eq. 6 is attributed to the physical process of grain growth (closing of the gaps present between grains) in the TF or possibly diffusion of cations in the smaller columnar grains. All data were fitted using this two process model in order to extract k_{Ex} values at all temperatures and oxygen partial pressures.

Figure 9 shows the logarithm of the surface exchange coefficient, k_{Ex}, as a function of $\log(p_{O_2})$ in the temperature interval 548–702°C. Also shown are values of k_{Ex} for a bulk sample. The values of k_{Ex} are plotted as a function of the end $\log(p_{O_2})$.

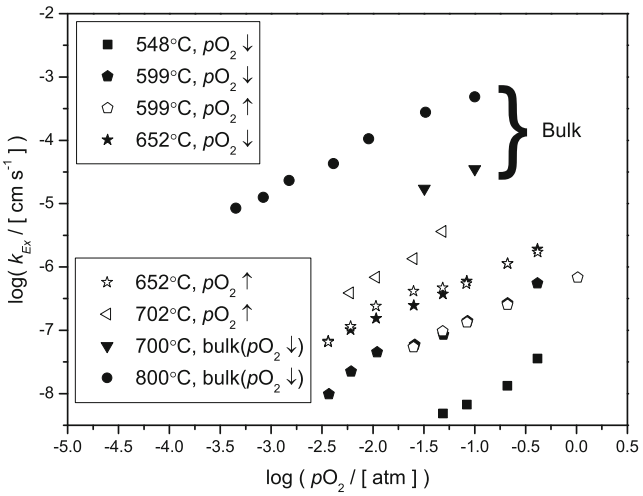

Fig. 9 Values of $\log(k_{Ex,1})$ (defined according to Eq. 6) as a function of $\log(p_{O_2})$ measured on LSF(c). *Open symbols* are for measurements performed under increasing p_{O_2} and *closed symbols* for decreasing p_{O_2}. Also shown are values obtained for a bulk sample [22]

From Fig. 9 it is observed that k_{Ex} decreases with decreasing p_{O_2} as also observed for bulk samples [16, 22]. Assuming that $k_{Ex} \propto p_{O_2}^n$ we get $n = 0.67$ and $n = 0.69$ at 599 and 652°C, respectively. The values of k_{Ex} determined from oxidation and reduction are almost the same when plotted as a function of the final p_{O_2}. This was also found by Chen et al. [9] for the composition $La_{0.5}Sr_{0.5}CoO_{3-\delta}$. We estimate the uncertainty on k_{Ex} to be 25%, originating mainly from the uncertainty in the fitting procedure. The finding that the surface exchange coefficient is the same, as long as the final p_{O_2} is the same indicates that sufficiently small steps in the p_{O_2} have been performed. If significantly larger steps were performed, the influence of the changes of defect concentrations (ie. electron holes, oxygen vacancies) would also contribute significantly to k_{Ex} as treated by Merkle and Maier [30].

At 700°C it is possible to compare the surface exchange parameters for the film and the bulk. It should be noted that it was only possible to measure two values of k_{Ex} for the bulk sample at 700°C due to the long relaxation times (~24 h). The values of k_{Ex} for bulk samples are significantly higher, by a factor of 6 ($p_{O_2} = 0.048$ atm), than the values for the TF. For LSF samples that have been thermally relaxed at 950°C, Mosleh et al. found values of k_{Ex} that are approximately two orders of magnitude smaller than what has been reported here. The reason for the higher values of k_{Ex} measured in this study compared to the thin film study of Mosleh et al. [14] can be assigned to the much larger electrochemically active surface area of the present investigated specimen given that this film has not been exposed to the higher temperatures leading to structural relaxation. Nevertheless, it seems that a tendency exists for LSF-TFs on MgO to exhibit significantly lower surface exchange parameters when compared to bulk specimens. The reason for this difference remains unknown, but a different surface composition or different facets than normally obtained for bulk samples could be at play. The activation energy of k_{Ex} for the film has been calculated to be (282 ± 20) kJ mol^{-1} ($p_{O_2} = 0.048$ atm). From a study of $(La_{0.6}Sr_{0.4})_{0.99}FeO_{3-\delta}$ on a bulk sample the activation energy was observed to be 199 ± 23 kJ mol^{-1} ($p_{O_2} = 8.7 \times 10^{-4}$ atm) [22]. Hence, also in terms of activation energies, the thin films deviate from bulk indicating that a different mechanism or a different step in the multi step incorporation reaction is rate limiting the oxygen incorporation. A number of speculations that can account for the observed results can be listed: (i) Recent studies indicate that strontium segregation to the surface of films prepared by PLD can have a very detrimental effect on the oxygen exchange kinetics [31]. (ii) As the films have been kept

at relatively low temperature, it is also possible that $SrCO_3$ have formed on the surface resulting in lower oxygen exchange coefficients. (iii) Strain in the films due to substrate—film interactions [32, 33] or (iv) The very small crystallite sizes can be speculated to lead to compositional differences at the surface that are different from that of the bulk.

5 Conclusion

Thin films of $(La_{0.6}Sr_{0.4})_{0.99}FeO_{3-\delta}$ on MgO substrates have been deposited by PLD. After deposition, the films were in a reduced state. Using a spectroscopic ellipsometer, the band gap of the reduced state was measured to be 2.1 eV. The electronic structure of the TF was found to be similar to that of the bulk material.

At 700°C the electrical conductivity of the film ($p_{O_2} = 0.048$ atm) was 26 S cm^{-1} compared to that for the bulk sample which is 180 S cm^{-1}, a reduction of the electrical conductivity by a factor of 7. The lower conductivity originates from the high effective porosity present in the TF, as the upper part of the film consists of columnar grains with gaps of a few nano-meters in between.

Using electrical conductivity relaxation, k_{Ex} as a function of p_{O_2} and temperature was determined. It was found that k_{Ex}, at a constant temperature, was a function of the final oxygen partial pressure, showing that the magnitude of the exchange coefficient was not influenced by changes in ionic defect concentrations. The values of k_{Ex} measured for thin films were demonstrated to be highly sensitive to the thermal annealing/history of the films and lower by a factor of 6 when compared to values measured for a bulk sample. Variations in surface chemistry and structure are suspected to be the cause of the difference.

Acknowledgements Harry Louis Tuller thanks the National Science Foundation under the Materials World Network (DMR 0908627) for its support. The views expressed in this article are not necessarily endorsed by the NSF.

References

1. R.T. Leah, N.P. Brandon, P. Aguiar, J. Power Sources **145**(2), 336 (2005)
2. Y.B. Matus, L.C. De Jonghe, C.P. Jacobson, S.J Visco, Solid State Ionics **176**(5–6), 443 (2005)
3. M.C. Tucker, G.Y. Lau, C.P. Jacobson, L.C. DeJonghe, S.J. Visco, J. Power Sources **175**(1), 447 (2008)
4. J. Januschewsky, M. Ahrens, A. Opitz, F. Kubel, J. Fleig, Adv. Funct. Mater. **19**(19), 3151 (2009)
5. D. Beckel, U.P. Muecke, T. Gyger, G. Florey, A. Infortuna, L.J. Gauckler, Solid State Ionics **178**(5–6), 407 (2007)
6. W. Jung, H.L. Tuller, Solid State Ionics **180**(11–13), 843 (2009)
7. P. Plonczak, A Bieberle-Hütter, M Søgaard, T. Ryll, J. Martynczuk, P.V. Hendriksen, L.J. Gauckler, Adv. Funct. Mater. **21**(14), 2764 (2011)
8. A. Bieberle-Hütter, M. Søgaard, H. Tuller, Solid State Ionics **177**(19–25), 1969 (2006)
9. X. Chen, S. Wang, Y.L. Yang, L. Smith, N.J. Wu, B.I. Kim, S.S. Perry, A.J. Jacobson, A. Ignatiev, Solid State Ionics **146**(3–4), 405 (2002)
10. I. Hole, T. Tybell, J.K. Grepstad, I. Wærnhus, T. Grande, K. Wiik, Solid-State Electron. **47**(12), 2279 (2003)
11. I. Wærnhus, *Defect Chemistry, Conductivity and Mass Transport Properties of* $La_{1-x}Sr_xFeO_{3-\delta}$ ($x = 0$ *and* $x = 0.1$). PhD-thesis, The Norwegian University of Science and Technology (2000)
12. F.S. Baumann, J. Fleig, H.U. Habermaier, J. Maier, Solid State Ionics **177**(11–12), 1071 (2006)
13. M. Mosleh, N. Pryds, P.V. Hendriksen, Mater. Sci. Eng. B **144**(1–3), 38 (2007)
14. M. Mosleh, M. Søgaard, P.V. Hendriksen, J. Electrochem. Soc. **156**(4), B441 (2009)
15. I. Yasuda, T. Hikita, J. Electrochem. Soc. **141**(5), 1268 (1994)
16. J.E. tenElshof, M.H.R. Lankhorst, H.J.M Bouwmeester, J. Electrochem. Soc. **144**(3), 1060 (1997)
17. C.R. Song, H.I. Yoo, Solid State Ionics, **124**(3), 289 (1999)
18. I. Yasuda, M. Hishinuma, J. Solid State Chem. **115**(1), 152 (1995)
19. J. Crank, *The Mathematics of Diffusion*, 1st edn. (Oxford University Press, Oxford, 1979)
20. I. Yasuda, M. Hishinuma, Solid State Ionics **80**(1–2), 141 (1995)
21. H.J.M. Bouwmeester, A.J. Burggraaf, in *The CRC Handbook of Solid State Electrochemistry*, eds. by P.J. Gellings, H.J.M. Bouwmeester (CRC Press, Boca Raton) (1997)
22. M. Søgaard, P.V. Hendriksen, M. Mogensen, J. Solid State Chem. **180**(4), 1489 (2007)
23. S.J. Litzelman, A. Rothschild, H.L. Tuller, Sens. Actuators B Chem. **108**, 231 (2005)
24. L.A. Chick, L.R. Pederson, G.D. Maupin, J.L. Bates, L.E. Thomas, G.J. Exarhos, Mater. Lett. **10**(1–2), 6 (1990)
25. M. Søgaard, P.V. Hendriksen, M. Mogensen, F.W. Poulsen, E. Skou, Solid State Ionics **177**(37–38), 3285 (2006)
26. P.V. Hendriksen, J.D. Carter, M. Mogensen, in *Proceedings of The Fourth International Symposium on Solid Oxide Fuel Cells (SOFC-IV)*, eds. by M. Dokiay, O. Yamamoto, H. Tagawa, S.C. Singhal, Electrochemical Society Proceedings, vol. 95–1 (Pennington, 1995) p. 934–943
27. P.H. Larsen, P.V. Hendriksen, M. Mogensen, J. Therm. Anal. **49**(3), 1263 (1997)
28. S.B. Adler, J. Am. Ceram. Soc. **84**(9), 2117 (2001)
29. A. Chainani, M. Mathew, D.D. Sarma, Phys. Rev. B **48**(20), 14818 (1993)
30. R. Merkle, J. Maier, Phys. Chem. **4**(17), 4140 (2002)
31. M. Kubicek, A. Limbeck, T. Fromling, H. Hutter, J. Fleig, J. Electrochem. Soc. **158**(6), B727 (2011)
32. J. Santiso, M. Burriel, J. Solid State Electrochem. **15**(5),985 (2011)
33. G.J. la O', S.-J. Ahn, E. Crumlin, Y. Orikasa, M.D. Biegalski, H.M. Christen, Y. Shao-Horn, Angew. Chem. **49**(31), 5344 (2010)